Journal of Molecular Structure 1200 (2020) 127047

Contents lists available at ScienceDirect

Journal of Molecular Structure

journal homepage: http://www.elsevier.com/locate/molstruc

Synthesis, *in vitro* cytotoxicity activity against the human cervix carcinoma cell line and *in silico* computational predictions of new 4-arylamino-3-nitrocoumarin analogues

Ahmed H. Halawa [a], Essam M. Eliwa [a, b, *], Ahmed A. Hassan [a, c], Hesham S. Nassar [a, d], R.A. El-Eisawy [a, d], Mohamed Ismail [b, e], Marcel Frese [b], Mohamed Shaaban [b, f], Ahmed M. El-Agrody [a, **], Ahmed H. Bedair [a], Norbert Sewald [b]

[a] Chemistry Department, Faculty of Science, Al-Azhar University, Nasr City-Cairo, 11884, Egypt
[b] Organic and Bioorganic Chemistry, Faculty of Chemistry, Bielefeld University, Bielefeld, D-33501, Germany
[c] Chemistry Department, Faculty of Science, Jazan University, Jazan, 82621, Saudi Arabia
[d] Chemistry Department, Faculty of Science and Art, Al-Baha University, Al-Baha, 1988, Saudi Arabia
[e] Microbiology Department, Faculty of Science, Helwan University, Helwan-Cairo, 11795, Egypt
[f] Chemistry of Natural Compounds Department, Pharmaceutical and Drug Industries Research Division, National Research Centre, El-Behoos St. 33, Dokki-Cairo, 12622, Egypt

ARTICLE INFO

Article history:
Received 8 July 2019
Received in revised form
5 September 2019
Accepted 7 September 2019
Available online 11 September 2019

Keywords:
4-Arylamino-3-nitrocoumarin
Cervical cancer
Cytotoxic activity
In silico computational predictions
Top1-DNA complex

ABSTRACT

A new series of 4-arylamino-3-nitrocoumarin analogues (**4**–**18**) have been synthesized and characterized by sophisticated spectroscopic techniques (^{1}H NMR, ^{13}C NMR) and mass spectrometry. All the new synthesized compounds were evaluated for their *in vitro* cytotoxic activity against the human cervix carcinoma cell line (KB-3-1) using resazurin assay with (+)-griseofulvin as the positive control ($IC_{50} = 19\ \mu M$). Among them, thiazolidinylidene derivative **17a** that bearing malononitrile unit displayed the best cytotoxic potency with IC_{50} value of 21 μM. Also, *in silico* docking simulation studies were conducted on human DNA topoisomerase 1 (Top1) (PDB: 1T8I) to explore and interpret the interaction pattern between the selected compounds and target enzyme as well confirm the acquired cytotoxicity results. In addition to the above, *in silico* predictions of physicochemical properties, ADME (absorption, distribution, metabolism and excretion) parameters, oral toxicity and indication of toxicity targets were implemented for some title compounds.

© 2019 Published by Elsevier B.V.

1. Introduction

Admittedly, cancer remains one of the most prevalent, knotted and fatal diseases in the present time. According to the World Health Organization (WHO) report in 2018, cancer is the second leading cause of death worldwide after heart disease, cancer burden rises to 18.1 million new cases and is responsible for an estimated 9.6 million deaths. About one in six deaths is due to cancer, so it emerges as a global epidemic. Nearly 70% of deaths from cancer take place in low- and middle-income countries (LMICs) [1]. Cervical cancer is caused by sexually gained infection with certain types of Human papillomavirus (HPV). Approximately all cases of cervical cancer can be attributable to HPV infection, smoking and HIV infection. Around the world, cervical cancer is the second most common cancer in women especially living in under developed regions with an estimated 570 000 new cases in 2018 representing 7.5% of all female cancer deaths. Among them, almost 311 000 women died from cervical cancer; more than 85% of these deaths occurring in LMICs and this number is projected to rise [2]. Thereby, there is an advantage and critically important in finding new anticancer agents with improved qualifications to gain better efficacy and selectivity as well low side effects.

Coumarin-containing derivatives are ubiquitous, versatile and endowed with a broad range of biological with pharmacological activities including anti-inflammatory [3], antioxidant [4], antifungal [5], antibacterial [6], anticoagulant [7], anticancer [8,9] and

* Corresponding author. Chemistry Department, Faculty of Science, Al-Azhar University, Nasr City-Cairo, 11884, Egypt.
** Corresponding author.
E-mail addresses: essameliwa85@azhar.edu.eg (E.M. Eliwa), elagrody_am@azhar.edu.eg (A.M. El-Agrody).

https://doi.org/10.1016/j.molstruc.2019.127047
0022-2860/© 2019 Published by Elsevier B.V.

anti-HIV [10,11]. Recently, a particular interest in thiazole−based compounds has been increased by researches attributable to their outstanding achievements in the prevention and curing of diseases [12−16]. Encouraged by the aforementioned findings and in line of our continuous research program, we synthesized and characterized new coumarin analogues incorporated with thiazole and other moieties. In addition to, we screened their *in vitro* cytotoxic activity against the human cervix carcinoma cell line (KB-3-1) using resazurin assay with (+)-griseofulvin as a positive control.

Indeed, *in silico* computational prediction approaches demonstrate an alternative and foster way for addressing the biological targets, molecular interaction mechanism of ligands with target protein and toxicity testing in the pharmaceutical industry and cosmetics, so these protocols play a crucial role for the progress in drug discovery and development [17]. In connection with biological targets, human topoisomerase 1 (Top1) is an enzyme that catalyze the cleavage and rejoining of a single strand of DNA, releasing the tension on the DNA twist and enabling DNA replication and/or mRNA transcription. Interfering with the Top1 would result in inhibition of cell replication and consequently cell death, thus it is recognized as an important target in human cancer tackling approaches [18,19]. Several naturally occurring and synthesized inhibitors classes were discovered and their mode of action has been characterized as potential antiproliferative agents. They work through the binding to the enzyme active site after the cleavage of the DNA backbone, inhibiting the religation step and accumulating Top1-DNA adduct [20]. Nevertheless, they suffer from low tumor response rates and dose limiting toxicity, therefore the search of inhibitors with higher activity is always desired. Accordingly, we shed light on the *in silico* computational studies encompassing the molecular docking of some synthesized 4-arylamino-3-nitrocoumarin derivatives as potential Top1-DNA inhibitors compared to the reference camptothecin (EHD) aiming to explore the binding affinity and key interactions between the synthesized ligands with target enzyme. Additionally, physicochemical properties, ADME parameters, acute oral toxicity and toxicity targets were predicted for some title compounds.

2. Materials and methods

2.1. Materials and instruments

Melting points were determined on a BÜCHI Melting Point B-540 apparatus and uncorrected (BÜCHI Germany). The NMR spectra (^{1}H NMR and ^{13}C NMR) were measured on Bruker Avance DRX 500 MHz (125 MHz for ^{13}C NMR) spectrometer (Bruker, USA) with TMS as an internal standard. Chemical shifts were reported relative to residual solvent peaks ([D_6]DMSO: ^{1}H: 2.50 ppm, ^{13}C: 39.5 ppm). ESI mass spectra were recorded using an ion trap mass spectrometer equipped with a standard ESI/APCI source (Bruker Daltonik GmbH, Bremen, Germany). Starting materials, reagents and solvents were obtained from commercial sources and used without further purification. The purity of the synthesized compounds was investigated by TLC, performed on Merck precoated silica gel 60 F_{254} aluminum sheets with solvent mixture of dichloromethane-methanol (95−5) as eluent. Spots were visualized under UV light at 254 nm. Elemental analyses were carried out at the Regional Centre for Mycology and Biotechnology (RCMP), Al-Azhar University, Cairo, Egypt.

2.2. Synthesis and characterization

2.2.1. 4-[(4-Acetylphenyl)amino]-3-nitrocoumarin (**4**)

The solution of 4-chloro-3-nitrocoumarin (**3**) (44 mmol) and *p*-aminoacetophenone (44 mmol) in ethanol (30 mL) in the presence of triethylamine (44 mmol) was refluxed for 4 h then cooled. The resulting solid was collected by filtration, washed with ethanol and recrystallized from dioxane to give compound **4** as a golden yellow crystals with a yield of 98% and Mp: 210−212 °C. NMR and MS data for all compounds are presented in supporting information file.

2.2.2. 2-{1-[4-((3-Nitrocoumarin-4-yl)amino)phenyl]ethylidene} hydrazinecarbothioamide (**5**)

A mixture of compound **4** (1 mmol) and thiosemicarbazide (1 mmol) in dioxane (10 mL) containing a catalytic amount of glacial acetic acid (1 mL) was heated under reflux for 3 h. The resulting solid on heating was collected by filtration, washed with hot ethanol and dried to afford compound **5** as a yellow amorphous solid with a yield of 87% and Mp: 248−250 °C.

2.2.3. 2-Cyano-N'-{1-[4-((3-nitrocoumarin-4-yl)amino)phenyl] ethylidene}acetohydrazide (**6**)

Compound **6** was generated as an orange amorphous powder from **4** in the same fashion that described for compound **5** with a yield of 98% and Mp: 274−276 °C.

2.2.4. 4-{[4-(2-Bromoacetyl)phenyl]amino}-3-nitrocoumarin (**7**)

To a stirred solution of **4** (0.02 mol) in warm glacial acetic acid (100 mL), the bromine (0.02 mol) was added dropwise with constant stirring in direct sun light for 5 h, then the reaction mixture was poured into crushed ice/water (100 g) with stirring. The separated solid was filtered off, washed with cold water, dried and recrystallized from dioxane to furnish **7** as a yellow amorphous solid with a yield of 95% and Mp: 236−238 °C.

2.2.5. General procedure for preparation of 4-{[4-(2-substituted-thiazol-4-yl)phenyl]amino}-3-nitrocoumarin (**8a-c**)

A mixture of **7** (1 mmol) and thiocarboxamide derivatives namely: (thiourea, phenyl thiourea, and thioacet-amide) (1 mmol) in dry dioxane (10 mL) containing TEA (1 mmol) was refluxed for 3 h. The resulting solid on heating was collected by filtration and washed with hot methanol to afford compounds **8a-c**.

4-{[4-(2-Aminothiazol-4-yl*)phenyl]amino}-3- nitrocoumarin* (8a) was obtained as a golden yellow amorphous powder with a yield of 80% and Mp: 338−340 °C.

4-{[4-(2-(Phenylamino)thiazol-4-yl*)phenyl]amino}-3-nitrocoumarin* (**8**b) was manifested as a yellow amorphous solid with a yield of 75% and Mp: 240−242 °C.

4-{[4-(2-Methylthiazol-4-yl*)phenyl]amino}-3-nitrocoumarin* (**8**c) was collected as an orange amorphous solid with a yield of 82% and Mp: 223−225 °C.

2.2.6. General procedure for preparation of 4-{[4-(2-(2-(4-substituted-benzylidene)hydrazinyl)thiazol-4-yl)phenyl]amino}-3-nitrocoumarin (**10a,b**)

In a similar vein, compounds **10a,b** were obtained as above-mentioned synthetic route for compounds **8a-c** by the reaction between **7** and benzylidene thiosemicarbazides namely: [1-(4-methoxybenzylidene)-thiosemicarbazide or 1-(4-chlorobenzylidene)thiosemicarbazide].

4-{[4-(2-(2-(4-Methoxybenzylidene)hydrazineyl)thiazol-4-yl*) phenyl]amino}-3-nitrocoumarin* (**10**a) was obtained as a yellow amorphous solid with a yield of 90% and Mp: 256−258 °C.

4-{[4-(2-(2-(4-Chlorobenzylidene)hydrazinyl)thiazol-4-yl*)phenyl] amino}-3-nitrocoumarin* (**10**b) was resulted as a golden yellow amorphous powder with a yield of 72% and Mp: 250−252 °C.

4-{[4-(Quinoxalin-2-yl)phenyl]amino}- 3-nitrocoumarin (**11**).

Compound **7** (1 mmol) and 1,2-phenylenediamine (1 mmol) were taken in dry dioxane (10 mL) containing TEA (1 mmol) and heated for 3 h under reflux. The reaction mixture was cooled to

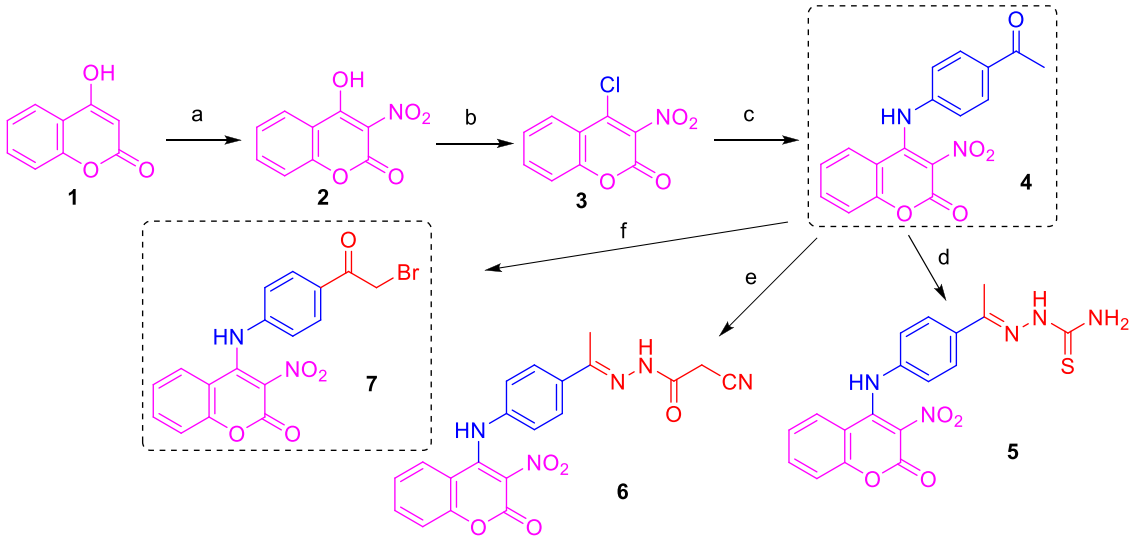

Scheme 1. Synthetic routes of compounds **4**–**7**. *Reagents and conditions*: (a) HNO_3/H_2SO_4, AcOH, rt, 2 h; (b) $POCl_3$, DMF, 10 °C then rt, 1 h; (c) *p*-aminoacetophenone, Et_3N, EtOH, reflux, 4 h; (d) thiosemicarbazide, AcOH, dioxane, reflux, 3 h; (e) cyanoacetohydrazide, AcOH, dioxane, reflux, 3 h; (f) Br_2, AcOH, rt, 5 h.

room temperature and methanol (5 mL) was added. The solid precipitate was filtered by suction, washed with hot methanol (10 mL) and dried to afford compound **11** as a yellow amorphous powder with a yield of 88% and Mp: 243–245 °C.

2.2.7. General procedure for preparation of *12* and *13*

A mixture of **7** (1 mmol) and heterocyclic amines namely: (2-aminopyridine or 2-aminopyrimidine) (1 mmol) in dry dioxane (10 mL) containing TEA (1 mmol) was refluxed for 2 h. The resulting solid on heating was collected by filtration, washed with hot methanol and dried to furnish compounds **12** and **13**, respectively.

4-{[4-(Imidazo[1,2-a]pyridin-3-yl)*phenyl]amino}-3-nitrocoumarin* (**12**) was demonstrated as a yellow amorphous powder with a yield of 87% and Mp: 278–280 °C.

4-{[4-(Imidazo[1,2-a]pyrimidin-3-yl)*phenyl]amino}-3-nitrocoumarin* (**13**) was accomplished as a reddish brown amorphous solid with a yield of 91% and Mp: 243–245 °C.

2.2.8. 4-{[4-(2-(1-Methylpiperazin-1-yl)acetyl)phenyl]amino}-3-nitrocoumain (*14*)

By the same token as stated above for **11**, compound **14** was produced from **7** (1 mmol) and 1-methylpiperazine (1 mmol) as a brown amorphous solid with a yield of 58% and Mp: 233–235 °C.

2.2.9. 4-{[4-(2-Thiocyanatoacetyl)phenyl]amino}- 3-nitrocoumarin (*15*)

A mixture of **7** (1 mmol) and potassium thiocyanate (1 mmol) in dry dioxane (10 mL) was refluxed for 2 h. The resulting solid on

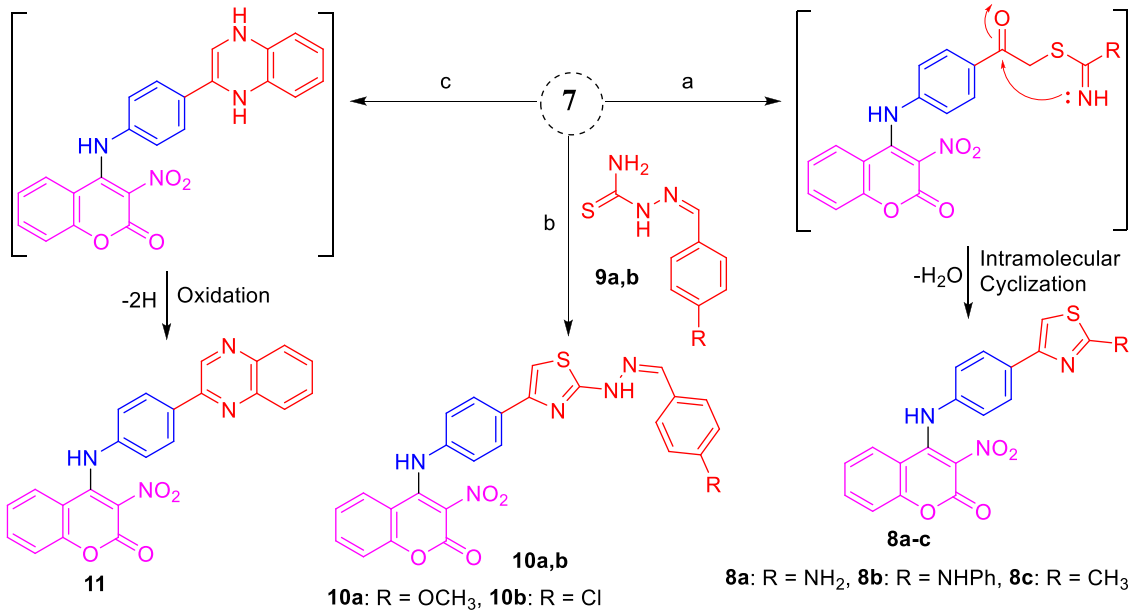

Scheme 2. Synthetic routes of compounds **8**–**11**. *Reagents and conditions*: (a) thiourea/phenyl thiourea/thioacetamide, Et_3N, dioxane, reflux, 3 h; (b) Et_3N, dioxane, reflux, 3 h; (c) 1,2-phenylenediamine, Et_3N, dioxane, reflux, 3 h.

heating was collected by filtration, washed with hot methanol and dried to donate compound **15** as a yellow amorphous solid with a yield of 85% and Mp: 208–210 °C.

*2.2.10. General procedure for preparation of **17a** and **18a***

Malononitrile or ethylcyanoacetate (1 mmol) was added to a stirred solution of potassium hydroxide (1 mmol) in anhydrous DMF (10 mL). Phenyl isothiocyanate (1 mmol) was added dropwise. The reaction mixture was stirred at room temperature with α-bromocarbonyl compound **7** (1 mmol) and left at room temperature for 6 h, then it was poured into ice/water and acidified with 0.1 N HCl. The resulting precipitate was filtered off, washed with water, dried and recrystallized from dioxane to afford compounds **17a** and **18a**, respectively.

2-(4-Hydroxy-4-(4-((3-nitro-2-oxo-2H-chromen-4-yl)amino) phenyl)-3-phenylthiazolidin-2-ylidene)malono-nitrile (**17a**) was proved as a golden yellow amorphous powder with a yield of 60% and Mp: 192–194 °C.

Eethyl-2-cyano-2-(4-hydroxy-4-(4-((3-nitro-2-oxo-2H-chromen-4-yl)amino)phenyl)-3-phenylthiazolidin-2-ylidene)acetate (**18a**) was indicated as a pale yellow amorphous powder with a yield of 91% and Mp: 284–286 °C.

2.3. In vitro cytotoxicity based upon resazurin assay

All the new synthesized compounds were evaluated for their *in vitro* cytotoxicity activity against the human cervix carcinoma cell line KB-3-1 (was obtained from the American Type Culture Collection, ATCC, Rockville, MD) according to our previously reported resazurin assay [21].

2.4. In silico docking study

Molecular dynamic simulation of some selected coumarin derivatives were built and energy minimized using Yet Another Scientific Artificial Reality Application (YASARA) [22]. The structure of human DNA Topoisomerase I was obtained from protein data bank (PDB code: 1T8I). The camptothecin inhibitor was removed, the missing hydrogens in the structure were added and the whole enzyme structure was energy minimized using AMBER14 force field, 10 Å cutoff and PME for long range electrostatics. Docking results were analyzed based on the B-factor (binding energy) that calculated by YASARA and correct positioning of the compounds within the active site of the enzyme. PyMol was used for the alignment study for the structures before and after simulation.

2.5. In silico predictions of physicochemical properties and ADME parameters

The physicochemical properties and ADME parameters of compounds **8a**, **10b**, **11** and **17a** in comparison with omeprazole drug were predicted using SwissADME web tool as described previously [23].

2.6. In silico acute oral toxicity prediction and indication of toxicity targets

The *in silico* prediction of rodent oral toxicity and indication of possible toxicity targets for compounds **8a**, **10b**, **11** and **17a** were implemented utilizing the ProTox web server as demonstrated by Drwal et al. [24].

3. Results and discussion

3.1. Chemistry

4-Hydroxycoumarin (**1**) was nitrated under mild condition to give 4-hydroxy-3-nitrocoumarin (**2**) that was treated with phosphorus oxychloride in DMF to form 4-chloro-3-nitrocoumarin (**3**) [25]. Reaction of **3** with *p*-aminoacetophenone afforded 4-[(4-acetylphenyl)amino]-3-nitrocoumarin (**4**). The ^{1}H NMR spectrum of **4** shows a singlet signal at δ 10.49 ppm that attributed to NH, also reveals multiplet signals between δ 8.38 and 7.32 ppm attributable to eight aromatic protons present in the molecule. In addition to, the acetyl group generated a singlet ^{1}H chemical shift at δ 2.58 ppm. The ^{13}C NMR spectrum of **4** displays a downfield ^{13}C resonance at δ 197.3 ppm for carbonyl acetophenoide and upfield one at δ 27.1 ppm for methyl carbon. ESI-MS spectrum of **4** exhibits the molecular ion peak at *m/z*: 347 $[M+Na]^+$ and 323 $[M-H]^-$.

Condensation of **4** with thiosemicarbazide and cyanoacetohydrazide gave the corresponding thiosemi-carbazone **5** and cyanoacetohydrazone **6** derivatives, respectively. The ^{1}H NMR spectrum of **5** indicate two singlet signal at δ 10.38 and 10.22 ppm attributable to 2NH. The ^{13}C NMR spectrum of **5** exhibits the absence of a carbonyl acetophenoide signal, while a downfield ^{13}C resonance at δ 179.2 ppm for the newly formed C=S group was appeared. Its ESI-MS spectrum manifests the molecular ion peak at *m/z*: 398 $[M+H]^+$, 420 $[M+Na]^+$ and 396 $[M-H]^-$. The NMR data of **6**

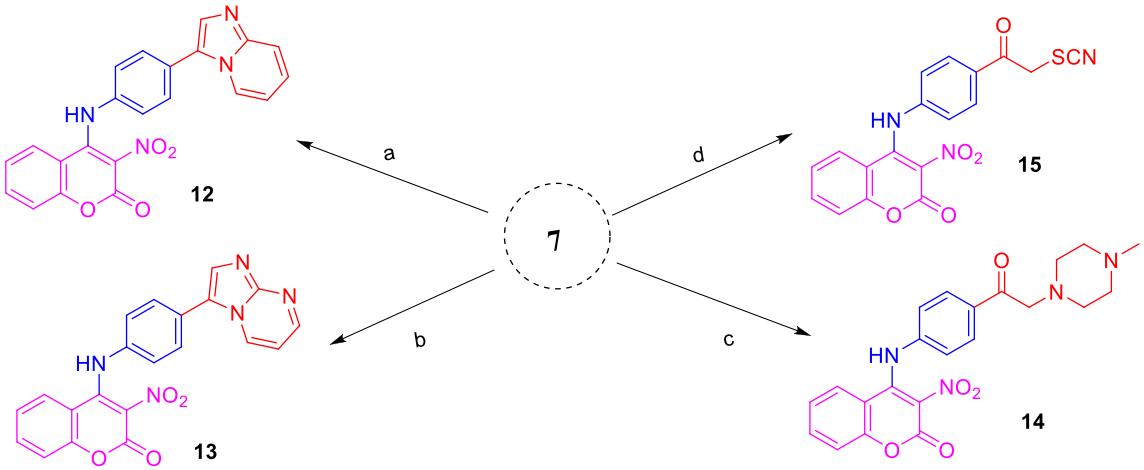

Scheme 3. Synthetic routes of compounds **12**–**15**. *Reagents and conditions*: (a) 2-aminopyridine, Et_3N, dioxane, reflux, 2 h; (b) 2-aminopyrimidine, Et_3N, dioxane, reflux, 2 h; (c) 1-methylpiperazine, Et_3N, dioxane, reflux, 3 h; (d) KSCN, dioxane, reflux, 2 h.

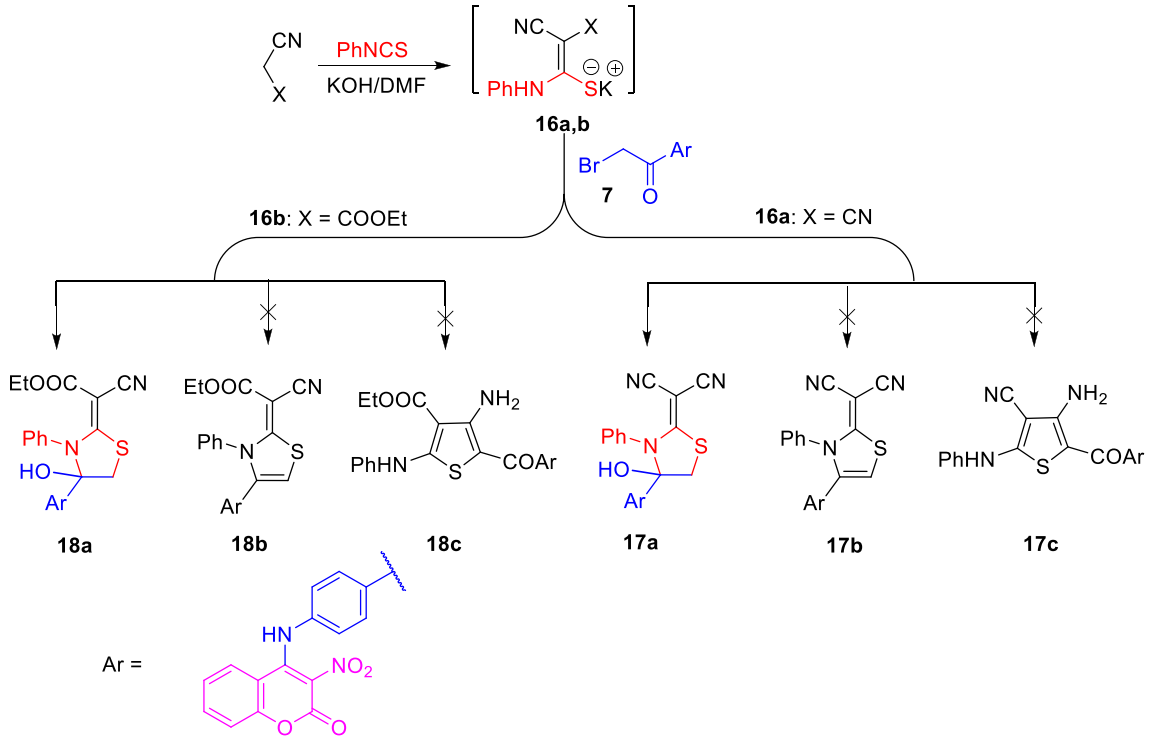

Scheme 4. Synthetic routes of compounds **17a** and **18a**.

Table 1
In vitro cytotoxicity of the synthesized compounds **4**–**18** against KB-3-1 cell line.

Compound	IC_{50} (μM)[a]	Compound	IC_{50} (μM)
	KB-3-1		KB-3-1
4	>100 ± 0.12	**11**	43 ± 0.6
5	–	**12**	–
6	–	**13**	–
7	>100 ± 0.5	**14**	–
8a	44 ± 0.4	**15**	>100 ± 0.12
8b	>100 ± 0.1	**17a**	21 ± 0.11
8c	>100 ± 0.2	**18a**	–
10a	–	(+)-Griseofulvin[b]	19.2 ± 0.03
10b	66 ± 0.02	DMSO[c]	–

[a] IC_{50} values expressed in μM as the mean values of triplicate wells from at least three experiments and are reported as the mean ± standard error.
[b] Positive control,[c] negative control, "–" means no obvious inhibitory effect.

Table 2
Binding affinity of different coumarin derivatives to Top 1 (PDB: 1T8I) and compared to the reference camptothecin (EHD).

Compound	Binding affinity (Kcal/mol)	No. of H-bonding
4	8.25	2
5	–	–
8a	8.44	3
10b	10.97	1
17a	10.09	2
EHD	9.48	4

"–" means no binding affinity or no H-bonding.

show a ^{1}H resonance at δ 4.29 for methylene protons and the respective methylene carbon at 25.4 ppm. As well, the carbonyl amide was demonstrated at δ 166.4 ppm. Synthesis of **7** was achieved by the reaction of **4** with bromine in glacial acetic acid (Scheme 1). The ^{1}H NMR spectrum of **7** exhibits ^{1}H resonance at δ 4.78 ppm that being for the newly formed methylene group, whilst the signal for methyl unit was disappeared. The ^{13}C NMR spectrum of **7** displays a ^{13}C chemical shift at δ 66.8 ppm attributable to the methylene carbon. (+)-ESI-MS spectrum of **7** indicates the molecular ion peaks at *m/z*: 425 $[M+Na]^+$ (94.92%, ^{79}Br) and 427 $[M+Na]^+$ (90.74%, ^{81}Br), (See supporting information Fig. S13).

The behavior of compound **7** towards thiocarboxamide derivatives was investigated. Thus, condensation of **7** with thiourea, phenyl thiourea and thioacetamide afforded the corresponding thiazolyl-3-nitrocoumarin derivatives **8a-c** [26] (Scheme 2). The ^{1}H NMR spectra of thiazole derivatives **8a-c** show a characteristic resonance of CH-thiazole at δ 7.25 for **8a**, 7.41 for **8b** and 7.99 ppm for **8c**. (+)-ESI-MS data for **8a-c** display the molecular ion peaks at *m/z*: 381 $[M+H]^+$ for **8a**, 479 $[M+Na]^+$ for **8b** and 402 $[M+Na]^+$ for **8c**, in agreement with the proposed empirical formulas. Moreover, reaction of **7** with benzylidene thiosemicarbazides **9a,b** [27] afforded the corresponding hydrazinyl thiazole derivatives **10a,b** (Scheme 2). The ^{1}H NMR spectra reveal the hydrazinyl-NH at δ 12.08 and coumarinyl-NH at 10.37 ppm for **10a**, also at δ 12.29 and 10.37 ppm, respectively, for **10b**. The CH-thiazole was defined at δ 7.38 for **10a** and 7.42 ppm for **10b**. The ^{13}C NMR data of **10a,b** display a downfield signal at δ 187.6 ppm attributable to thiazolyl C=N that flanked by three heteroatoms. (+)-ESI-MS spectra for **10a,b** show the molecular ion peaks at *m/z*: 536 $[M+Na]^+$ for **10a** and 540 $[M+Na]^+$ (100%, ^{35}Cl) with 542 $[M+Na]^+$ (35%, ^{37}Cl) for **10b**. Further, reaction of **7** with 1,2-phenylenediamine yielded the corresponding quinoxalinyl-3-nitrocoumarin derivative **11**. The formation of **11** is explained by cyclocondensation of **7** with 1,2-phenylenediamine, followed by subsequent oxidation [26]. The ^{1}H NMR spectrum **11** discloses the absence of 2NH group that characteristic for 1,4-dihydroquinoxaline derivative, meanwhile it shows a ^{1}H chemical shift at δ 10.49 ppm attributable to coumarinyl-NH and another one at δ 9.64 ppm that assignable for CH-quinoxaline. The ESI-MS spectrum of **11** represents the molecular ion peak at *m/z*: 433 $[M+Na]^+$ and 409 $[M-H]^-$.

Our investigation was extended to include the behavior of **7**

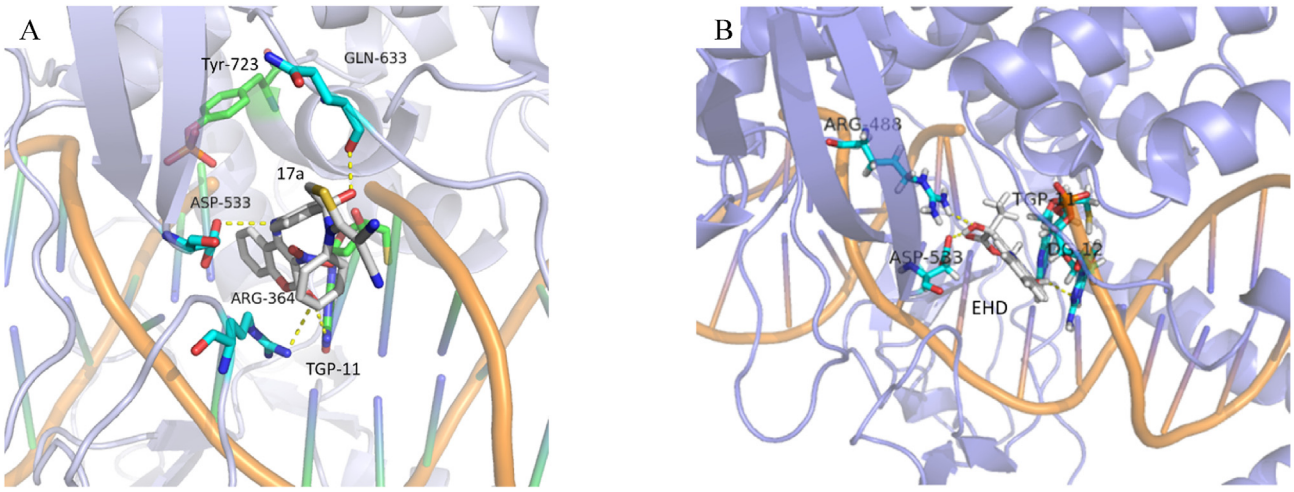

Fig. 1. A) esidues (cyan) Predicted binding mode of compound **17a** (grey) and B) the reference compound EHD (grey) within the active site of the Top1-DNA complex (PDB: 1T8I), showing the interaction of the inhibitors with the amino acid rof the enzyme and DNA base pair.

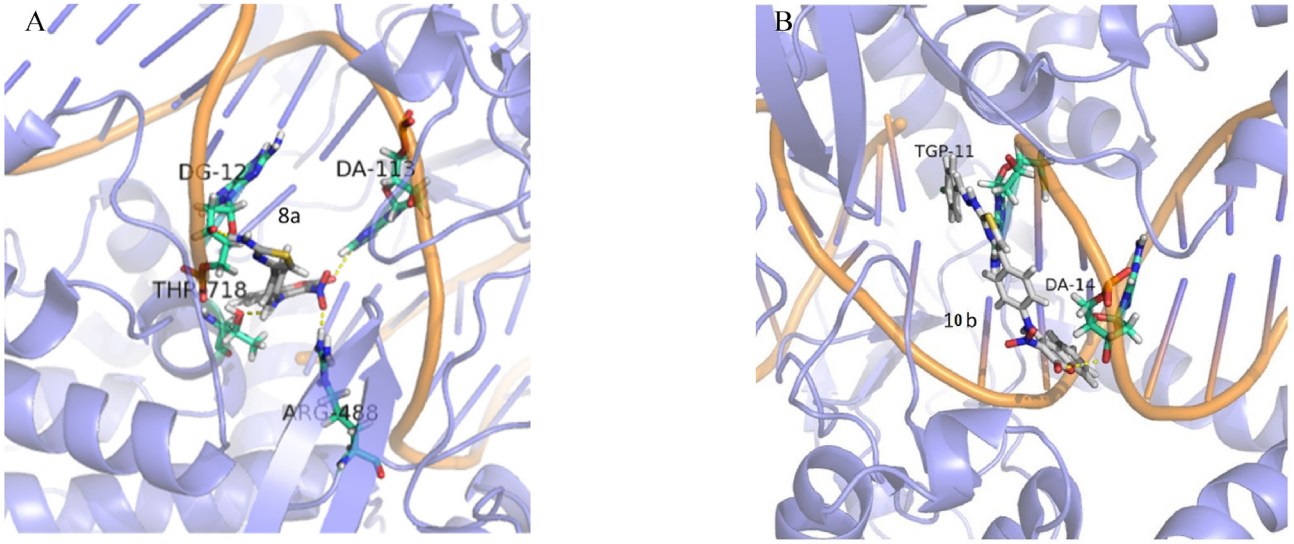

Fig. 2. A) Predicted binding mode of compounds **8a** and B) **10b** within the active site of Top1 (PDB: 1T8I). Hydrogen bondings are shown in yellow dashed lines. DNA backbone is shown in orange and Top 1 in slate.

towards another heterocyclic amines to build different fused heterocyclic rings. Thus, treatment of compound **7** with different amines namely: (2-amino-pyridine and 2-aminopyrimidine) afforded the corresponding derivatives **12**, and **13**, respectively (Scheme 3). The ^{1}H NMR spectra manifest the absence of a characteristic signal to methylene protons, while display a singlet one attributable to the newly formed CH-imidazole at δ 8.82 for **12** and 8.66 ppm for **13**. (+)-ESI-MS spectra for **12** and **13** show the molecular ion peaks at *m/z*: 399 $[M+H]^+$ and 400 $[M+H]^+$, respectively. Furthermore, nucleophilic substitution reaction of **7** with 1-methylpiperazine gave the expected product 1-methylpiperazinyl-3-nitrocoumain derivative **14** (Scheme 3). The ^{1}H NMR spectrum of **14** generates the CH_2-piperazine chemical shift at δ 3.17 ppm. The corresponding carbon resonance was detected by ^{13}C NMR spectrum at δ 51.1, whilst 49.1 ppm was attributed to methyl carbon. (+)-ESI-MS spectrum of **14** shows the molecular ion peak at *m/z*: 423 $[M+H]^+$. Direct reaction of equimolar amounts from **7** with potassium thiocyanate according to S_N2 mechanism yielded the corresponding coumarinyl thiocyanato derivative **15** [26]. Its ^{13}C NMR spectrum exhibits CN resonance at δ 115.1 ppm. The ESI-MS spectra of **15** represent the molecular ion peaks at *m/z*: 404 $[M+Na]^+$ in positive mode and 380 $[M-H]^-$ in negative mode, establishing the molecular weight of **15** as 381 Da.

Finally, active methylene reagents such as malononitrile or ethylcyanoacetate was treated with phenyl isothiocyanate in DMF containing potassium hydroxide to afford the non-isolable intermediates **16a,b** that treated directly with **7** to give the corresponding thiazolidinylidene derivatives **17a** and **18a**, respectively. The synthetic pathway for thiazole derivatives (**17b**, **18b**) or thiophene derivatives (**17c**, **18c**), as reported by Fadda et al. [28] or Abdelhamid and Al-Shehri [29], respectively, was failed in our practice (Scheme 4). The structure of **17a** was deduced by the ^{1}H NMR spectrum that indicates the thiomethylene diastereotopic *geminal* coupling protons (J = 12.4 Hz) at δ 4.12 and 3.82 ppm (See supporting information Fig. S45). Also, ESI-MS spectra of **17a** show the molecular ion peak in positive mode at *m/z*: 546 $[M+Na]^+$ and 522 $[M-H]^-$ in negative mode. The ^{1}H NMR spectrum of **18a** exhibits triplet and quartet *vicinal* protons (J = 7.1 Hz)

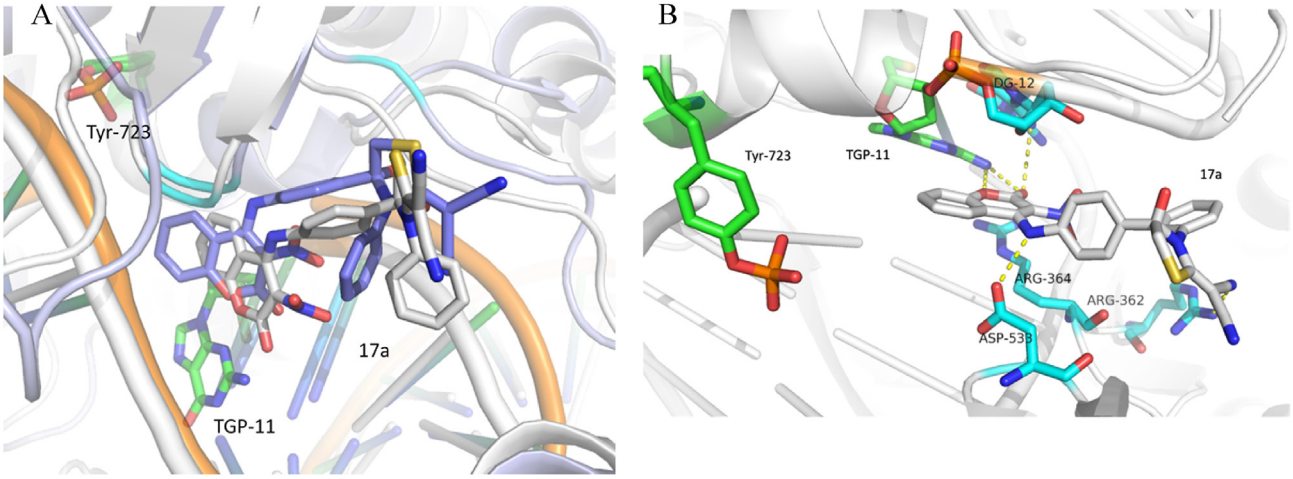

Fig. 3. A) Superimposed Top1 structure (PDB: 1T8I) before (blue) and after simulation (grey) with docked compound **17a** before MD simulation (blue) and after 1 ns simulation (grey); B) an internal view of the active site pocket with the structural deviation of **17a** showing the H-bonding (yellow dots) with the Top1 amino acid residues (cyan and green).

at δ 4.12 and 1.17 ppm, respectively, attributable to the ester group, as well shows *geminal* protons ($J = 12.6$ Hz) at δ 3.84 and 3.57 ppm that attributed to CH_2S fragment. The ^{13}C NMR spectrum of **18a** displays the corresponding ester carbons at δ 60.5 and 14.8 ppm, respectively.

3.2. Cytotoxicity activity evaluation by resazurin assay

The *in vitro* cytotoxicity activity of the new synthesized compounds **4**–**18** were evaluated against KB-3-1 cell line using resazurin-based assay [21] with (+)-griseofulvin as the positive control. As appeared in Table 1, thiazolidinylidene derivative **17a** that containing malononitrile fragment exhibited the best cytotoxic

Table 3
Physicochemical Properties, drug-likeness and lead-likeness parameters of compounds **8a**, **10b**, **11** and **17a** in comparison with omeprazole drug.

Predictive models and their parameters	Compounds				
	8a	10b	11	17a	Omeprazole
Physicochemical Properties					
MW	380.38 g/mol	517.94 g/mol	410.38 g/mol	523.52 g/mol	345.42 g/mol
Fraction Csp3	0.00	0.00	0.00	0.07	0.29
RB[a]	4	7	4	5	5
H-bond acceptors	5	6	6	7	5
H-bond donors	2	2	1	2	1
MR[b]	106.36	144.45	119.38	147.25	93.70
TPSA[c]	155.21 Å^2	153.58 Å^2	113.84 Å^2	184.41 Å^2	96.31 Å^2
Lipophilicity					
Log $P_{o/w}$[d] (XLOGP3)	4.11	7.03	4.71	4.93	2.23
Log $P_{o/w}$ (WLOGP)	4.16	6.48	5.06	4.61	3.61
Water Solubility					
Log S[e] (ESOL)	−5.10	−7.57	−5.71	−6.29	−3.52
Qualitative solubility	Moderately soluble	Poorly soluble	Moderately soluble	Poorly soluble	Soluble
Drug-likeness					
Lipinski (RO5)[f]	Yes; 0 violation	Yes; 1 violation: MW > 500	Yes; 0 violation	Yes; 1 violation: MW > 500	Yes; 0 violation
Ghose[g]	Yes	No; 3 violations: MW > 480, WLOGP>5.6, MR > 130	Yes	No; 2 violations: MW > 480, MR > 130	Yes
Veber[h]	No; 1 violation: TPSA>140	No; 1 violation: TPSA>140	Yes	No; 1 violation: TPSA>140	Yes
Bioavailability Score	0.55	0.55	0.55	0.55	0.55
Lead-likeness					
Rule of three (RO3)[i]	No; 2 violations: MW > 350, XLOGP3>3.5	No; 2 violations: MW > 350, XLOGP3>3.5	No; 2 violations: MW > 350, XLOGP3>3.5	No; 2 violations: MW > 350, XLOGP3>3.5	Yes

[a] RB = Rotatable bonds.
[b] MR = Molar Refractivity.
[c] TPSA = Topological polar surface area.
[d] Log $P_{o/w}$ = The partition coefficient between *n*-octanol and water.
[e] Log S = The decimal logarithm of the molar solubility in water.
[f] Lipinski (RO5) criteria range are: lipophilicity (Log $P_{o/w}$) ≤ 5, MW ≤ 500, H-bond donors ≤ 5 and H-bond acceptors ≤ 10.
[g] Ghose filter criteria range are: Log $P_{o/w}$ in −0.4 to +5.6 range, MR from 40 to 130, MW from 180 to 480, No. of atoms from 20 to 70.
[h] Veber rule criteria range are: RB ≤ 10 and TPSA ≤140 Å^2.
[i] RO3 criteria range are: XLOGP3 ≤ 3.5, MW ≤ 350, H-bond donors ≤3, H-bond acceptors ≤3 and RB ≤ 3 [23,30].

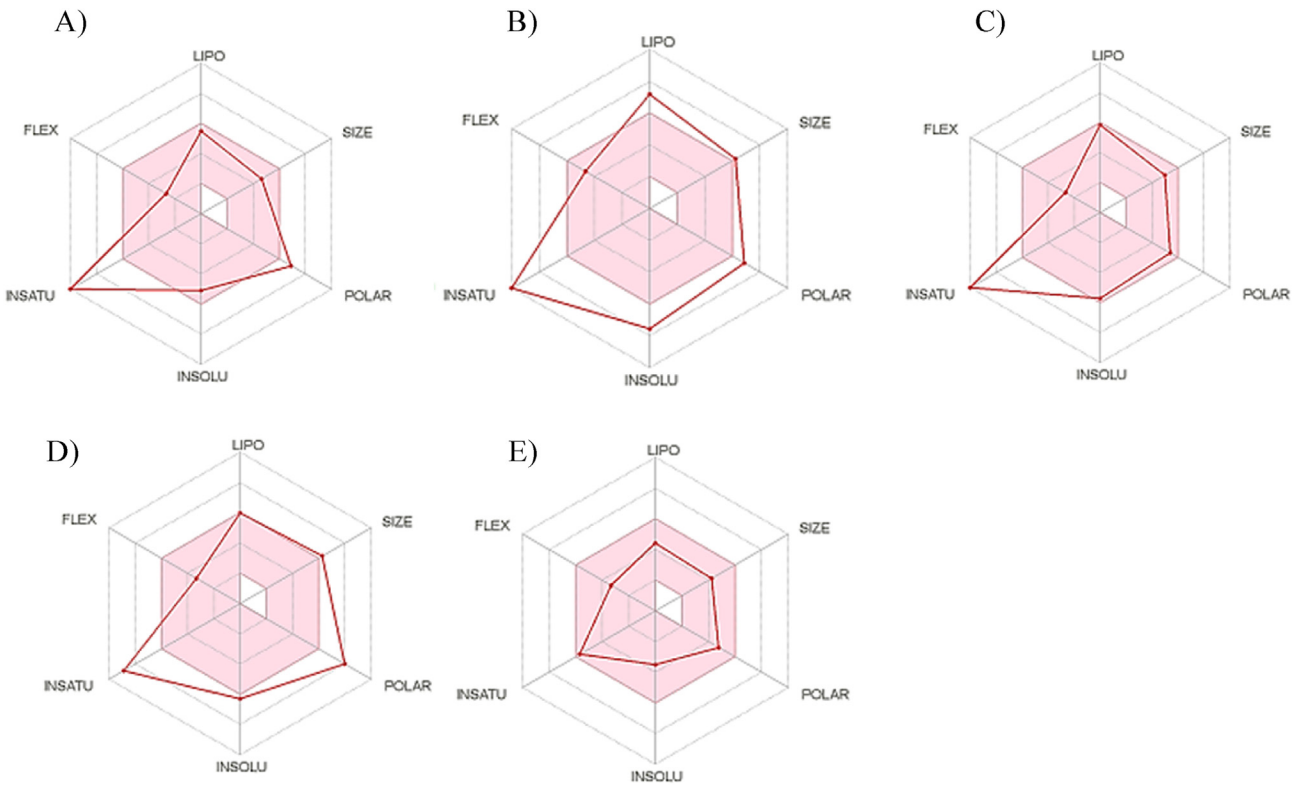

Fig. 4. Bioavailability Radar plot of the predicted compounds: A) for **8a**; B) for **10b**; C) for **11**; D) for **17a**; E) for omeprazole drug. The pink area shows the optimal range for each properties (Lipophilicity: XLOGP3 between −0.7 and + 5.0, size: MW between 150 and 500 g/mol, polarity: TPSA between 20 and 130 Å^2, solubility: log S not higher than 6, saturation: fraction of carbons in the sp^3 hybridization not less than 0.25, and flexibility: no more than 9 rotatable bonds) [23].

Table 4
Pharmacokinetics parameters of compounds **8a**, **10b**, **11** and **17a** in comparison with omeprazole drug.

Pharmacokinetics parameters	Compounds				
	8a	10b	11	17a	Omeprazole
GI (HIA) absorption[a]	Low	Low	Low	Low	High
BBB permeant[b]	No	No	No	No	No
P-gp substrate[c]	No	No	No	No	Yes
CYP1A2 inhibitor	Yes	No	No	No	Yes
CYP2C19 inhibitor	Yes	Yes	No	Yes	Yes
CYP2C9 inhibitor	Yes	No	Yes	Yes	Yes
CYP2D6 inhibitor	No	No	Yes	No	Yes
CYP3A4 inhibitor	Yes	No	No	Yes	Yes
Log K_p[d] (skin permeation)	−5.70 cm/s	−4.47 cm/s	−5.46 cm/s	−5.99 cm/s	−6.82 cm/s

[a] GI (HIA) = Human gastrointestinal absorption.
[b] BBB = Blood-brain barrier permeation.
[c] P-gp = Permeability glycoprotein.
[d] Log K_p = The skin permeability coefficient.

potency with IC_{50} value of 21 μM and very close to the reference [(+)-griseofulvin IC_{50} = 19.2 μM], whereas thiazolyl derivatives **8a** and **10b** as well quinoxalinyl analog **11** showed moderate activity with IC_{50} values 44, 66 and 43 μM, respectively. On the other hand, derivatives **4**, **7**, **8b**, **8c** and **15** indicated lower activity with IC_{50} values over than 100 μM, whilst compounds **5**, **6**, **10a**, **12**, **13**, **14** and **18a** showed no activity toward KB-3-1. In general, the results suggested that compound **17a** have potent antiproliferative and cytotoxic activity against KB-3-1but limited unfavorable effects on normal cells.

3.3. Docking study

Docking analysis of some selected synthesized coumarin-based scaffolds possessing different IC_{50} values to Top1 enzyme as an effective target for cancer treatment was carried out [22]. As represented in Table 2, docking results revealed that, the potential antiproliferative activity of these compounds compared to the reference camptothecin (EHD) – a known Top1 inhibitor, where compound **17a** that have the highest cytotoxicity activity, showed high binding affinity of 10.09 kcal/mol to the Top1-DNA complex, despite the bulky structure of the compound, it can access the active site, forming important H-bonds with Arg364, Asp533, Gln633 and 5′-Thio-2′-deoxyguanosine phosphonic acid of the DNA backbone (TGP11); besides the Pi stacking stabilizing the potential inhibitor. Coumarin unit of **17a** is directed within the active site between the catalytic 3-phosphotyrosine (Tyr723) and 5-phosphothiolate (TGP11) of the DNA backbone that might hinder

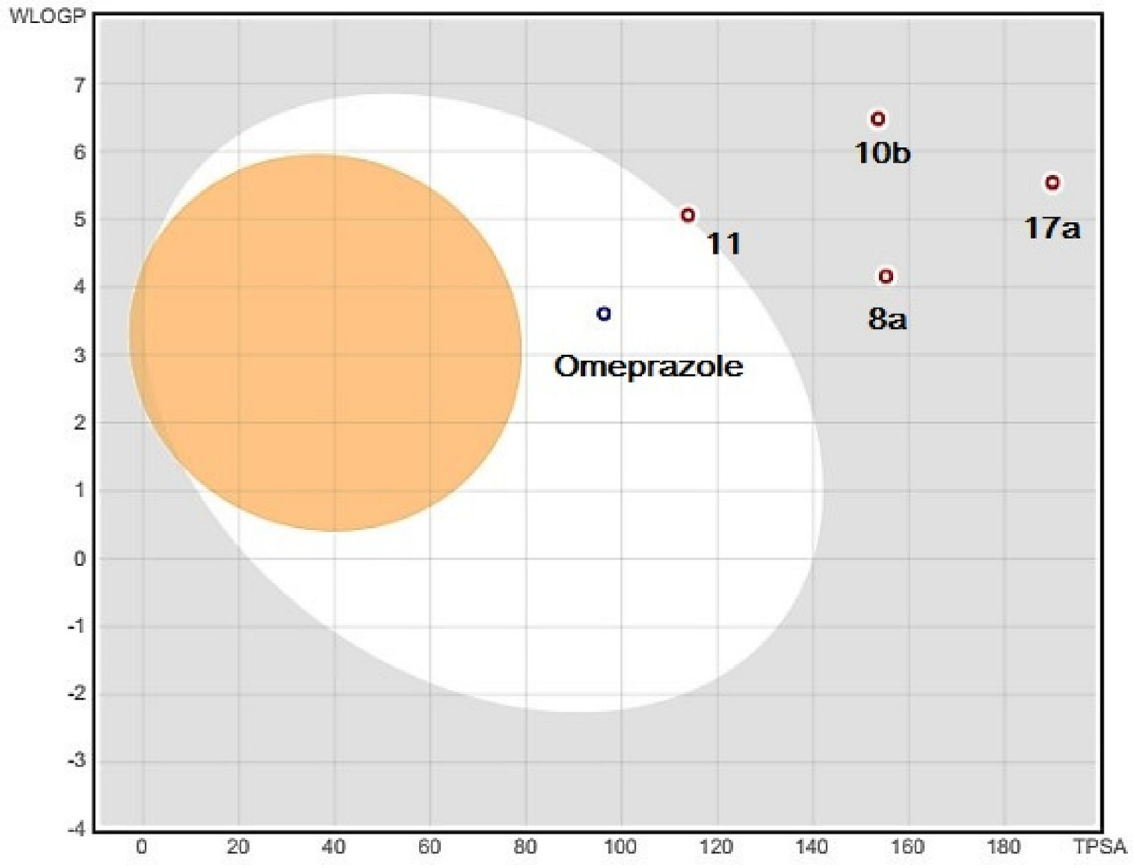

Fig. 5. The BOILED-Egg plot of the predicted compounds **8a**, **10b**, **11** and **17a** in comparison with omeprazole drug. The white region is for highly probable HIA (GI) absorption, and the yellow region (yolk) is for highly probable BBB permeation. The outside grey region stands for molecules are predicted with low absorption and not brain penetration. As well, the points are colored in blue if predicted as P-gp substrate (PGP+) and in red if predicted as P-gp non-substrate (PGP−) [23,31].

Table 5
In silico oral toxicity prediction and indication of toxicity targets for compounds **8a**, **10b**, **11** and **17a**.

Compound	Predicted LD_{50} (mg/kg)	Predicted Toxicity Class[a]	Average similarity (%)	Prediction accuracy (%)	Toxic fragments	Binding to toxicity targets
8a	300	3	39.77	23	Nil	No
10b	1000	4	37.59	23	Nil	No
11	1000	4	41.29	54.26	Nil	No
17a	1000	4	35.87	23	Nil	No

[a] Toxicity Class ranging from 1 to 6 according to the Global Harmony System (GHS) [24].

the second transesterification required for rejoining DNA backbone. On the other hand, camptothecin displayed slightly lower binding affinity (9.48 kcal/mol) than **17a**, however four H-bonds with Asp533, Arg488 and two DNA base pair were formed besides the base stacking interaction (Fig. 1).

Thiazolyl derivative **8a** with relatively low IC_{50} value 44 μM, exhibited lower binding affinity (8.44 kcal/mol) than **17a** and EHD, in spite of it formed three H-bonds with the enzyme and DNA backbone. Surprisingly, the 4-chlorobenzylidene hydrazinyl thiazolyl analog **10b** with IC_{50} value 66 μM, manifested the highest binding affinity (10.97 kcal/mol), although only one H-bond was detected with the DNA backbone, but three pi stacking could be recognized with the DNA backbone that explain the strong binding and stability of the compound. So, the low IC_{50} value may be attributable to low accessibility of **10b** through the cell membrane (Fig. 2). Compound **4** with $IC_{50} > 100$ showed low binding energy (8.25 kcal/mol) besides it correlated away from the catalytic 3-phospotyrosine. As the cytotoxicity result, no binding affinity within the active site of the Top1 was observed for compound **5**.

In order to further investigate the potentiality of compound **17a** as a Top1 inhibitor, molecular dynamic (MD) simulation was employed. Interestingly, **17a** was more oriented within the active site pocket of Top 1 that enabled H-bond formation with residues Arg362, Arg364, Asp533 and 5′-Thio-2′-deoxyguanosine phosphonic acid (TGP11) and 2′-Deoxyguanosine 5′-monophosphate (DG12) from the DNA backbone (Fig. 3). In the same manner, MD simulation was conducted on the reference compound EHD, but no more deviation was observed after 1 ns of the simulation time with retention of the same interactions pattern to Top 1-DNA complex (four H-bonding with Lys532, Asp533, Arg488 and Arg364).

3.4. Physicochemical properties and ADME parameters

To our delight by the findings obtained from cytotoxicity screening and docking study, we used SwissADME web tool as described previously [23] to predict the physicochemical properties

and ADME parameters of compounds **8a**, **10b**, **11** and **17a** in comparison with omeprazole drug that conforms to Lipinski's rule of five (RO5). As stated in Table 3, these compounds passed the filter of Lipinski's rule with zero violation for **8a** and **11**, whereas compounds **10b** and **17a** passed with one violation attributable to the molecular weight that over than 500 g/mol. Consequently, these compounds have oral bioavailability.

Interestingly, compound **11** passed the filter of both Ghose and Veber rules without any violation like omeprazole drug. Besides, all the predicted compounds as well omeprazole drug displayed the same bioavailability Score (0.55). For defining lead-likeness, our predicted compounds share the same violations to the rule of three (RO3) attributable to MW > 350 and XLOGP3>3.5. In that regard, the Bioavailability Radar planner is displayed for a rapid evaluation of drug-likeness taken into account six physicochemical inspections including lipophilicity, size, polarity, solubility, flexibility and saturation (Fig. 4) [23]. The pink area indicates the range of optimal values for each parameter. Obviously, all the predicted compounds from the first glance showed deviation particularly the highly unsaturation degree (Fraction Csp3 = 0.0), leading to suboptimal physicochemical properties for oral bioavailability, whilst also omeprazole drug displayed all the properties in the optimal range (pink area). Moreover, solubility is one pioneer property affecting the absorption [23] and concerning qualitative water solubility, all the predicted compounds ranged from poorly to moderately soluble based on ESOL topological model, but omeprazole drug was soluble.

With regard to the pharmacokinetic behaviors, the estimation of our predicted compounds to be substrate or non-substrate of the permeability glycoprotein (P-gp) and to be inhibitor or non-inhibitor of the most important cytochromes P450 isoenzymes (CYP1A2, CYP2C19, CYP2C9, CYP2D6, CYP3A4), was implemented by the support vector machine algorithm (SVM) model [23]. As shown in Table 4, omeprazole drug inhibited the different CYP isoenzymes, while our evaluated compounds manifested selectivity for particular isoforms, for instance, compound **8a** suppressed four types among them: CYP1A2, CYP2C19, CYP2C9 and CYP3A4, but compound **10b** only affected CYP2C19. As well, **17a** inhibited three CYP isoforms: CYP2C19, CYP2C9 and CYP3A4. Noteworthy, CYP2D6 isoenzyme was only affected by quinoxalinyl-3-nitrocoumarin derivative **11**.

Based on BOILED-Egg model (WLOGP *vs* TPSA) that illustrated in Fig. 5 [23,31], all the tested compounds demonstrated low GI absorption, not brain penetration and P-gp non-substrates (PGP-, red dots), while omeprazole drug was predicted high absorbed, but not BBB permeant and PGP+ (blue dot). Importantly as well, predicting the skin permeability coefficient (K_p) of our chemical compounds and omeprazole was done as described by Potts and Guy [32], where the more negative the log K_p, the less skin permeant is the compound. Also essential, Log K_p depends upon the molecular size (MW) and lipophilicity (Log $P_{o/w}$) of chemical compound and predicted by this algorithm: Log K_p (cm/s) = −6.3 + 0.71* Log $P_{o/w}$ (XLOGP3) − 0.0061* MW [32].

3.5. Oral toxicity prediction and indication of toxicity targets

In our practice, we utilized the ProTox web server to estimate rodent oral toxicity and indication of possible toxicity targets for compounds **8a**, **10b**, **11** and **17a** as reported previously [24]. Concerning oral toxicity, this technique predicts by comparison of input molecule two-dimensional structure with similar dataset compounds that have known median lethal doses (LD_{50}) values measured in rodents and determination of toxic fragments. With regard to toxicity targets, this approach also shows of possible toxicity targets based upon the similarity of input compound to known ligands of that protein target and the ligand mapping to pharmacophores models (Toxicophores). As tabulated in Table 5, the evaluated LD_{50} was ranged from 300 to 1000 mg/kg for the predicted compounds. The higher the LD_{50}, the lower toxic effect is the molecule. Our tested molecules were predicted to toxicity classes 3 or 4 and have not any toxic fragments. Also, all these compounds are non-binding to toxicity targets.

4. Conclusions

In summary, a new series of 4-arylamino-3-nitrocoumarin derivatives were synthesized starting from 4-hydroxycoumarin and characterized by various spectral methods. All the compounds were subjected for *in vitro* cytotoxicity activity against KB-3-1 cancer cell line. Compound **17a** exhibited a promising activity in the tested compounds. The docking and MD simulation study provide an additional evidence for the potentiality and possible interaction mechanism of the new coumarin derivatives as antiproliferative agents targeting Top1-DNA complex and hence as anticancer agents. As well, *in silico* prediction of physicochemical properties and oral toxicity manifested that compound **17a** passed the filter of Lipinski's rule and have low toxic effect, respectively. So, compound **17a** would become a valuable lead for additional investigation. Also, compounds **5** and **6** will be utilized as a starting material for further modification.

Conflicts of interest

The authors declare that they have no conflict of interest.

Acknowledgements

The authors are grateful to the NMR and MS Departments at Bielefeld University for spectral measurements. We would like to thank Carmela Michalek for biological activity testing and Marco Wißbrock with Anke Nieß for technical assistance. This research work has been financed by the German Academic Exchange Service (DAAD) with funds from the German Federal Foreign Office in the frame of the Research Training Network "Novel Cytotoxic Drugs from Extremophilic Actinomycetes" (Project ID57166072).

Appendix A. Supplementary data

Supplementary data to this article can be found online at https://doi.org/10.1016/j.molstruc.2019.127047.

References

[1] https://www.who.int/news-room/fact-sheets/detail/cancer, accessed on 2018-09-12.
[2] https://www.who.int/en/news-room/fact-sheets/detail/human-papillomavirus-(hpv)-and-cervical-cancer, accessed on 2019-01-24.
[3] Z. Li, J. Hu, M. Sun, H. Ji, S. Chu, G. Liu, N. Chen, Anti-inflammatory effect of IMMLG5521, a coumarin derivative, on Sephadex-induced lung inflammation in rats, Int. Immunopharmacol. 14 (2012) 145–149.
[4] A.H. Halawa, A.A. Hassan, M.A. El-Nassag, M.M. Abd El-All, G.A. Abd El-Jaleel, E.M. Eliwa, A.H. Bedair, Synthesis, reactions, antioxidant and anticancer evaluation of some novel Coumarin derivatives using ethyl 2-(2-oxo-4-phenyl-2*H*-chromen-7-yloxy)acetate as a starting material, Eur. J. Chem. 5 (2014) 111–121.
[5] E. Valadbeigi, S. Ghodsi, Synthesis and characterization of some new thiazolidinedione derivatives containing a coumarin moiety for their antibacterial and antifungal activities, Med. Chem. 7 (2017) 178–185.
[6] Y. Shi, C.-H. Zhou, Synthesis and evaluation of a class of new coumarin triazole derivatives as potential antimicrobial agents, Bioorg. Med. Chem. Lett 21 (2011) 956–960.
[7] O.M. Abdelhafez, K.M. Amin, R.Z. Batran, T.J. Maher, S.A. Nada, S. Sethumadhavan, Synthesis, anticoagulant and PIVKA-II induced by new 4-hydroxycoumarin derivatives, Bioorg. Med. Chem. 18 (2010) 3371–3378.
[8] H. Zhao, B. Yan, L.B. Peterson, B.S.J. Blagg, 3-Arylcoumarin derivatives manifest

anti-proliferative activity through Hsp90 inhibition, ACS Med. Chem. Lett. 3 (2012) 327–331.
[9] M.A.I. Salem, M.I. Marzouk, A.M. El-Kazak, Synthesis and characterization of some new coumarins with *in vitro* antitumor and antioxidant activity and high protective effects against DNA damage, Molecules 21 (2016) 249–269.
[10] J.R. Hwu, R. Singha, S.C. Hong, Y.H. Chang, A.R. Das, I. Vliegen, E. De Clercq, J. Neyts, Synthesis of new benzimidazole-coumarin conjugates as anti-hepatitis C virus agents, Antivir. Res. 77 (2008) 157–162.
[11] J. Neyts, E. De Clercq, R. Singha, Y.H. Chang, A.R. Das, S.K. Chakraborty, S.C. Hong, S.-C. Tsay, M.-H. Hsu, J.R. Hwu, Structure-activity relationship of new anti-hepatitis C virus agents: heterobicycle-coumarin conjugates, J. Med. Chem. 52 (2009) 1486–1490.
[12] O.I. El-Sabbagh, M.M. Baraka, S.M. Ibrahim, C. Pannecouque, G. Andrei, R. Snoeck, J. Balzarini, A.A. Rashad, Synthesis and antiviral activity of new pyrazole and thiazole derivatives, Eur. J. Med. Chem. 44 (2009) 3746–3753.
[13] V. Zaharia, A. Ignat, N. Palibroda, B. Ngameni, V. Kuete, C.N. Fokunang, M.L. Moungang, B.T. Ngadjui, Synthesis of some p-toluenesulfonyl-hydrazinothiazoles and hydrazino-bis-thiazoles and their anticancer activity, Eur. J. Med. Chem. 45 (2010) 5080–5085.
[14] I. Hutchinson, S.A. Jennings, B.R. Vishnuvajjala, A.D. Westwell, M.F.G. Stevens, Antitumor benzo-thiazoles: synthesis and pharmaceutical properties of antitumor 2-(4-aminophenyl)benzothiazole amino acid prodrugs, J. Med. Chem. 45 (2002) 744–747.
[15] F. Azam, B.A. El-gnidi, I.A. Alkskas, M.A. Ahmed, Design, synthesis and anti-Parkinsonian evaluation of 3-alkyl/aryl-8-(furan-2-yl)thiazolo[5,4-e][1,2,4]triazolo[1,5-c]pyrimidine-2(3H)-thiones against neuro-leptic-induced catalepsy and oxidative stress in mice, J. Enzym. Inhib. Med. Chem. 25 (2010) 818–826.
[16] R.N. Sharma, F.P. Xavier, K.K. Vasu, S.C. Chaturvedi, S.S. Pancholi, Synthesis of 4-benzyl-1,3-thiazole derivatives as potential anti-inflammatory agents: an analogue-based drug design approach, J. Enzym. Inhib. Med. Chem. 24 (2009) 890–897.
[17] P.K. Vuppala, D.R. Janagam, P. Balabathula, Importance of ADME and bio-analysis in the drug discovery, J. Bioequiv. Availab. 5 (2013) 1–2.
[18] J.J. Champoux, DNA TOPOISOMERASES: structure, function, and mechanism, Annu. Rev. Biochem. 70 (2001) 369–413.
[19] Y. Pommier, Drugging topoisomerases: lessons and challenges, ACS Chem. Biol. 8 (2013) 82–95.
[20] D.M. Shadrack, V.M.K. Ndesendo, Molecular docking and ADMET study of emodin derivatives as anticancer inhibitors of NAT2, COX2 and TOP1 enzymes, Cell. Mol. Bioeng. 7 (2017) 1–18.
[21] A.H. Halawa, S.M. Abd El-Gilil, A.H. Bedair, E.M. Eliwa, M. Frese, N. Sewald, M. Shaaban, A.M. El-Agrody, Synthesis of diverse amide linked bis-indoles and indole derivatives bearing coumarin-based moiety: cytotoxicity and molecular docking investigations, Med. Chem. Res. 27 (2018) 796–806.
[22] G.M. Morris, D.S. Goodsell, R.S. Halliday, R. Huey, W.E. Hart, R.K. Belew, A.J. Olson, Automated docking using a lamarckian genetic algorithm and empirical binding free energy function, J. Comput. Chem. 19 (1998) 1639–1662.
[23] A. Daina, O. Michielin, V. Zoete, SwissADME: a free web tool to evaluate pharmacokinetics, drug-likeness and medicinal chemistry friendliness of small molecules, Sci. Rep. 7 (2017) 42717–42730.
[24] M.N. Drwal, P. Banerjee, M. Dunkel, M.R. Wettig, R. Preissner, ProTox: a web server for the in silico prediction of rodent oral toxicity, Nucleic Acids Res. 42 (2014) W53–W58.
[25] B.R. Dekić, N.S. Radulović, V.S. Dekić, R.D. Vukićević, R.M. Palić, Synthesis and antimicrobial activity of new 4-heteroarylamino coumarin derivatives containing nitrogen and sulfur as heteroatoms, Molecules 15 (2010) 2246–2256.
[26] H.M. Mohamed, A.H.F. Abd El-Wahab, K.A. Ahmed, A.M. El-Agrody, A.H. Bedair, F.A. Eid, M.M. Khafagy, Synthesis, reactions and antimicrobial activities of 8-ethoxycoumarin derivatives, Molecules 17 (2012) 971–988.
[27] A.H. Halawa, Synthesis, reactions and biological evaluation of some novel 5-bromobenzofuran-based heterocycles, vol. 2, 2014, pp. 9–17. W. J. O. C.
[28] A.A. Fadda, M.M. Mukhtar, H.M. Refat, Utility of activated nitriles in the synthesis of some new heterocyclic compounds, AJO (Am. J. Ophthalmol.) C. 2 (2012) 32–40.
[29] A.O. Abdelhamid, S.M. Al-Shehri, A convenient synthesis of thiophene, 13-thiazole, 2.3-Dihydro-1.3.4-thiadiazole and pyrazole derivatives, J. Chem. Res. (1997) 240–241.
[30] K.F.M. Atta, O.O.M. Farahat, T.Q. Al-Shargabi, M.G. Marei, T.M. Ibrahim, A.A. Bekhit, E.H. El Ashry, Syntheses and in silico pharmacokinetic predictions of glycosylhydrazinyl-pyrazolo[1,5-c]pyrimidines and pyrazolo[1,5-c]triazolo[4,3-a]pyrimidines as anti-proliferative agents, Med. Chem. Res. 28 (2019) 215–227.
[31] A. Daina, V. Zoete, A BOILED-egg to predict gastrointestinal absorption and brain penetration of small molecules, ChemMedChem 11 (2016) 1117–1121.
[32] R.O. Potts, R.H. Guy, Predicting skin permeability, Pharm. Res. 9 (1992) 663–669.